

11-1-2017

Optical Properties of Organic Carbon and Soot Produced in an Inverse Diffusion Flame

C. Russo

Istituto di Ricerche sulla Combustione

B. Apicella

Istituto di Ricerche sulla Combustione

J. S. Lighty

Boise State University

A. Ciajolo

Istituto di Ricerche sulla Combustione

A. Tregrossi

Istituto di Ricerche sulla Combustione

Publication Information

Russo, C.; Apicella, B.; Lighty, J. S.; Ciajolo, A.; and Tregrossi, A. (2017). "Optical Properties of Organic Carbon and Soot Produced in an Inverse Diffusion Flame". *Carbon*, 124, 372-379. <http://dx.doi.org/10.1016/j.carbon.2017.08.073>

Optical properties of organic carbon and soot produced in an inverse diffusion flame

C. Russo^{a*}, B. Apicella^a, J.S.Lighty^b, A. Ciajolo^a and A.Tregrossi^a

a. Istituto di Ricerche sulla Combustione, CNR, Piazzale Tecchio, 80, 80125 Napoli, Italy.

b. Department of Mechanical and Biomedical Engineering, Boise State University, Boise, ID, United States.

Research Paper

**Corresponding author*

Telephone number: +39 081 768 22 54

E-mail: carmela.russo@irc.cnr.it

Abstract

The carbonaceous matter (soot plus organic carbon) sampled downstream of an ethylene inverse diffusion flame (IDF) was chemically and spectroscopically analyzed in detail. In particular, the H/C ratio, the UV-Visible absorption coefficient and Raman parameters were measured and found to be representative of a highly disordered sp^2 -rich carbon as the early soot sampled in a premixed flame. In contrast, the optical band gap was found to be relatively low (0.7eV), closer to the optical band gap of graphite than to that of medium-sized polycyclic aromatic hydrocarbons (>2eV) which are widely considered to be soot precursors and are mostly contained in the organic carbon. The significance of the optical band gap as signature of different structural levels (nano-, micro- and macro-structure) of sp^2 -rich aromatic disordered carbons was critically analyzed in reference to their molecular weight/size distribution. The relevance of the optical band analysis to the study of the soot formation mechanism was also highlighted.

1. Introduction and background

The classification of disordered (non-crystalline) carbon materials with sp^2 -bonding as polyaromatic solids [1] or, more recently, as graphenic carbon materials [2], traces them to the structural elements of the carbon network, namely polycyclic aromatic hydrocarbons (PAH) and graphene layers, respectively. PAH molecules of different size and shape have been considered as molecularly defined subunits of graphite [3] and, more recently, as monodisperse “mini-subunits” of graphene [4]. Hence, polyaromatic and graphenic terms can be used interchangeably envisioning PAH as small flakes of graphene with hydrogen atoms at the edges. Assemblies of two-dimensional more or less developed polyaromatic or graphenic systems are considered as the basic structural units of disordered sp^2 -bonded carbons as char, coke, soot, etc. It is worth noting that the piling of graphene/polyaromatic layers in these materials determines the occurrence, often simultaneous, of the so called 0D order (amorphous), 2D order (turbostratic, i.e. randomly stacked) and 3D order (crystalline) [5].

Interestingly, PAH are a leitmotif joining the so-called organic carbon, (also named soluble organic fraction, tar, condensed species, etc.) constituted of individual small ($>C_{10}$) and large PAH molecules ($>C_{24}$) with the solid carbon (soot, black carbon, elemental carbon, etc.). Organic carbon and soot together constitute the carbonaceous particulate matter present in atmospheric aerosols that are produced in fires or emitted from combustion systems used for energy production, transport, heating, etc.. The physico-chemical properties of combustion-derived carbon particles (size, composition, amount of absorbed organic carbon, etc.) are important for determining their value for practical applications as well as their impact on the environment, air quality and human health [6,7]. For example, the optical properties of soot, i.e., light absorption and scattering, have important effects on the earth's radiative balance and, hence, on climate change [8]. In addition, the optical properties of soot are also used as diagnostics for measuring heat transfer in fires and combustion aerosols [9], and even for identifying the composition of interstellar matter using soot as a carbon analogue [10-12].

In early pioneering research, specific optical properties of soot, namely the dispersion exponent [13-15] and the absorption coefficient [16] were proven to be valuable signatures of soot structure. Optical properties have also been exploited more recently for evaluating soot aging, aerosol composition and the response of optical diagnostics based on laser light absorption for soot measurements [9, 17-21]. Strictly correlated to the optical dispersion is the optical band gap, a parameter commonly used in solid-state physics for predicting applicability and performance of solid materials in optoelectronic devices, and also used for evaluating the aromatic characteristics (size, aromatic content) of non-crystalline carbons. Generally, the optical gap for non-crystalline

(organic and inorganic) materials is empirically defined either as the E₀₄ gap, the energy at which the optical absorption coefficient $\alpha = 10^4 \text{ cm}^{-1}$, or by using the equation $(\alpha E)^n = B(E - E_g)$ where B is a constant, E is the photon energy ($E = h\nu$) of the incident light, and E_g is the band gap. In particular, if $(\alpha E)^n$ vs E is a straight line at the absorption edge, down to the visible-near infrared (NIR) range, then E_g can be obtained from the extrapolation to energy axis. Actually, this equation derives from the semi-empirical expression independently derived by Tauc [22] and Davis–Mott [23] where the exponents $n=0.5$ and $n=2$ are considered to typify indirect and direct transitions, respectively.

The Tauc equation ($n=0.5$) has been mostly used for determining the band gap of that class of non-crystalline carbon materials, customarily named amorphous carbons [24, 25], composed of small units of planar polyaromatic layer (cluster) embedded in a sp^3 matrix. The standard sp^2 -bonded cluster model suggested by Robertson [24, 25] has been considered valid for this kind of carbon materials [24] with the cluster size determining the optical band gap [25]. Actually, non-crystalline carbons having hydrogen as a ternary element include a wide variety of materials with a dependence on the sp^3 and sp^2 bond types and hydrogen content, the main parameters representative of their variability. The typical ternary phase diagram of non-crystalline carbon [26-29] is reported in Figure 1 where soot, precursors and some reference molecules have been added to the various forms of amorphous carbons [28]. As noticed by Ferrari and Robertson [30], the ternary diagram is not totally comprehensive of the structural variability of non-crystalline carbons because another parameter should be added as a “fourth dimension”, the degree (size) of clustering of the sp^2 phase. To this regard, the optical band gap, with some assumptions on structure and shape, could be directly related to the cluster’s size [24]. Following Robertson’s study, many others have shown that the Tauc equation offers the best fit to the optical absorption data of the majority of non-crystalline carbons [10, 31-36].

Compact clusters of fused six-fold rings featuring PAH are considered to rule the optical band gap of amorphous carbons. In particular, it has been proposed that the optical band gap is inversely proportional to the diameter of a circular cluster (or to the square root of the number of aromatic rings in a cluster), and thereby to the aromatic layer length associated [24, 25].

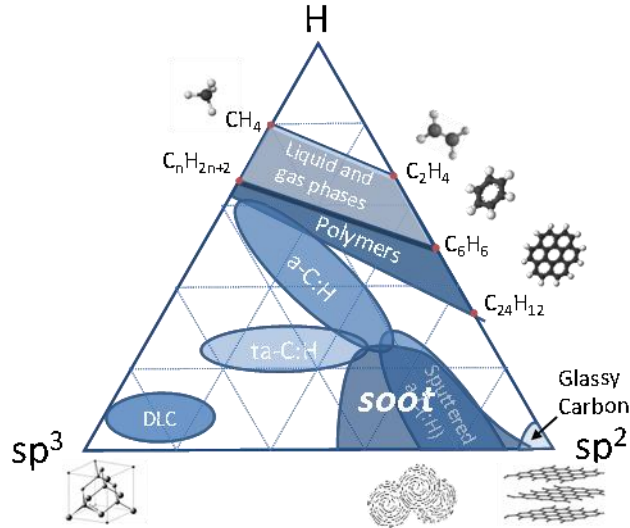


Figure 1 Ternary diagram of carbon showing sp^3 , sp^2 and H content of amorphous carbons (a-C, PD a-C:H ta-C:H), soot and reference molecules (adapted from Refs. 26-29).

The Eg concept, first introduced in combustion by Minutolo et al. [37], has been exploited for the study of the flame-formed soot structure and composition [38-43] as well as for describing the absorption characteristics of atmospheric carbon particles produced from combustion [44]. The Eg measured on the UV-Visible (UV-Vis) spectra of flame-sampled soot [38-40] showed values quite low ($<1\text{eV}$) corresponding to aromatic layer lengths larger than those obtained by HR-TEM lattice fringe analysis. It is worthy to note that even though soot can be considered a polycrystalline material, the crystallite size is centered around 1nm with a small spread of values as shown in previous work reporting the aromatic fringe distributions [45]. Moreover, large aromatic layer lengths are in contrast with the vision of the soot internal structure as constituted of small polyaromatic layers, instead characterized by high band gaps (2-4 eV) [41, 46], more or less (turbostratically) stacked together. This model of soot structure has been postulated on the basis of chemical [47] and modeling [48] works, and also, more recently derived from HRTEM [45, 49-51] and Raman [45, 52, 53] measurements.

Discrepancies between the lengths of the aromatic layers calculated with Eg and those measured through high-resolution transmission electron microscopy (HRTEM) analysis have been found for sp^2 -hybridized carbon materials as carbon nanoparticles produced from laser ablation of graphite [32-34]. Such discrepancies can lead to the belief that the procedure for deriving the Eg from the absorption spectra can fail and/or Eg could have a quite different physical meaning, if any, when applied to of highly disordered sp^2 -rich carbonaceous materials.

Definitely, some specific features of the absorption spectra have to be considered in interpreting the band gap of non-crystalline carbons, as the absorption edge broadening, due to the presence of clusters with different morphologies, sizes and distortions, leads to a distribution of local gaps. In the case of carbons almost totally constituted of sp^2 -bonded carbon, such as sputtered carbons [24, 25], the absorption coefficient, replotted in the Tauc domain, fits a linear function over limited spectral portions of the UV-Vis range. Different values of E_g can then be obtained by extrapolating different parts of the absorption curve [25]. This is also the case of the extinction spectra measured inside fuel-rich sooting flames where diverse E_g have been evaluated and attributed to differently-sized aromatic absorbers featuring soot precursors and soot particles [37].

Notably, it has been found that the extinction spectra measured before soot inception show a unique contribution in the UV range, due to chromophores with high E_g (between 3 and 4eV) associated to small size (two- to four-rings) PAH. As soon as soot is formed, i.e. in nearly-sooting conditions, there is an abrupt increase in the visible absorption, associated with low E_g (<1eV) [37]. The sudden appearance of visible absorption and low E_g , typically associated to large aromatic sizes, are not consistent with the idea of a progressive aromatic size growth during soot formation; also it is unexpected in view of the large contribution of gas-phase and/or externally-mixed small-sized PAH, having high optical band gaps, which are abundantly present at soot inception. Remarkably, relatively high optical band gap values (around 2eV), corresponding to moderately-sized PAH layers, could be evaluated in a narrow spectral region (440-540nm) of the extinction spectra measured in diffusion flames through the traditional Tauc plot calculated by using $n=0.5$ in the Tauc-Davis Mott equation [41]. Similar values of optical band gaps have been measured in a smaller wavelength range (420-490nm) by using $n=2$, but the $(\alpha E)^2$ vs E plot did not exhibit the same degree of linearity [42].

Both high (around 2eV) and low E_g values (<1eV) have been evaluated by using a multiple band gap spectral fitting of the UV-Vis spectra of soot probed by batch sampling and thermophoretic methods in premixed flames [38-40]. Indeed, low E_g values (<1eV) have been observed even for the so-called “young” soot, i.e. soot formed early in the flame, before massive soot growth and graphitization take place [40]. This could be due to some contamination with few mature soot particles featured by sp^2 clusters of larger size since E_g is not dominated by the aromatic layers/clusters of average size, but by the larger or less compact (even few) clusters [24, 25]. The interference from mature soot could occur because of some overlap of the soot inception and growth regions in atmospheric pressure premixed and diffusion flames. The inverse diffusion flame (IDF) is a configuration recognized as source of freshly-formed soot [54-58] as compared to a traditional diffusion flame. In the IDF, fuel flows in the outer annulus versus the inner, resulting in

precursor and soot being formed and immediately transported to the non-reactive region of the flame. Because of the inherent high flow rates of precursor species passing almost intact throughout the reaction zone, the IDF is the flame configuration suitable for providing both organic carbon and highly-disordered soot which should retain the chemical and morphological features of the flame-formed precursors.

Following a preliminary comparison of the chemical and spectroscopic properties of soot (young and mature) sampled in a premixed ethylene flame and downstream of an ethylene IDF, the present work focuses on the UV-Vis spectroscopic analysis of the IDF carbon particulate (soot plus organic carbon), with the specific aim of analyzing the significance of the optical band gap as signature of structural features of highly disordered sp^2 -rich carbons.

2. Experimental

The IDF burner was designed after the system of Blevins et al. [54]. The flow rates of air, fuel, and nitrogen were 5 SLPM, 15 SLPM, and 60 SLPM, respectively. The visible flame height in a dark room was 60 mm. Two replicates of carbon particulate matter samples were taken at 10 cm above the tip of the flame using a 10-cm-length stainless steel probe with a 1mm-i.d. capillary tip. The probe was constructed using the design of Zhao et al. [59] and Kasper et al. [60] and was connected to a 0.25- μ m Teflon filter to collect bulk carbon particulate matter including condensates at 40 °C (the operating temperature of the heating tape). The organic compounds condensed and/or adsorbed on the solid carbon (soot) were separated by solubilization in dichloromethane (DCM). Both the organic compounds dissolved in DCM, hereafter named organic carbon, and soot were recovered for the spectroscopic characterization. PAH constituting the organic carbon were identified by gas chromatography-mass spectrometry (GC-MS). Soot was ultrasonically suspended in *n*-methylpyrrolidinone (NMP) and further separated on an Anotop filter (Whatman) to isolate the soot fraction with particle diameter <20nm. UV-Vis and fluorescence spectra of carbon samples were respectively measured on a HP 8453 diode array spectrophotometer and on a PerkinElmer LS-50 spectrofluorometer. Raman spectra were measured by means of a Horiba XploRA Raman microscope system (Horiba Jobin Yvon, Japan) with an excitation wavelength of $\lambda = 532$ nm.

Size Exclusion Chromatography (SEC) was carried out on a HP1050 chromatograph eluting the DCM-extract and soot with NMP and measuring on-line UV-Vis spectra of the molecular weight (MW)-segregated fractions from 250nm up to 600nm by means of a diode array detector. The MW/size calibration curve was built on polystyrene standards and on carbonaceous samples with size measured by Dynamic Light Scattering [61]. The MW distribution of dry soot was measured in a wide MW range (1E5-1E11u) by using a “non-porous” column, whereas the lighter and more

abundant PAH components of the DCM-soluble fraction were analyzed in the 100-1E5u range on a highly cross-linked “individual-pore” polystyrene/divinyl benzene column to get the MW distribution of the DCM-soluble fraction [39, 40, 61, 62].

3. Results and Discussion

The main properties of the IDF soot sample are reported in Table 1 in comparison with those of soot sampled in a premixed ethylene/O₂ flame (PMX, C/O=0.8, cold gas velocity=4 cm/s) at 6 mm (young PMX) and 10mm (mature PMX) of height above the burner. The results show the similarities of IDF and young PMX soot. First, their organic carbon/soot mass ratio is high and very similar (Table 1). Moreover, both young PMX and IDF soot samples show a relatively high H/C atomic ratio (0.2) and a low visible mass absorption coefficient (around 2m²/g at 500nm) rather different from those of mature PMX soot [17-19]. Eventually, a high sp² content (about 90%) was evaluated for all soot samples on the basis of FT-IR analysis method set up on soot [63] and recently developed for determining the sp²-content of coal tar pitch [62]. High sp² contents (>80%) have been also typically measured by electron energy loss spectroscopy (EELS) for diesel soot [65, 66] and for young and mature flame-derived soot (our unpublished data).

Table 1 Main properties of soot collected in ethylene PMX and IDF flames

Property	PMX soot mature	PMX soot young	IDF soot
organic carbon/soot, g/g	0.35	1.14	0.92
H/C	0.09	0.19	0.22
Mass specific absorption @300nm, m ² /g	8.11	3.16	4.73
Mass specific absorption @500nm, m ² /g	4.57	1.80	2.01
I(D)/I(G)	0.88	0.75	0.74
FWHM (G), cm ⁻¹	68.50	50.20	51.60
Optical band gap (Tauc), eV	0.17	0.5	0.7

The high sp² content and low hydrogen value (Table 1) trace the IDF as well as the PMX soot samples to the specific class of highly-disordered carbons like chars, glassy carbon, sputtered carbon [27], diesel soot, and carbon black [65, 66], all confined in the lower right hand corner of the ternary carbon diagram (Figure 1). Beside their intrinsic complexity, the structural description of such disordered carbon materials is not easily achievable due to the fact that the low hydrogen content limits the use of important analytical tools like NMR, FTIR, etc.. As well, the “fourth

dimension” important to infer the carbon structure at the molecular level [30], namely the sp^2 cluster size, is difficult to determine reliably.

A careful deconvolution procedure of the Raman spectra has been recently used for evaluating as the cluster size changes during soot formation in premixed flames of diverse fuels [53]. This procedure well reconstructs the Raman spectra of the IDF and PMX soot reported in Figure 2 in comparison with the spectrum reconstructed for the young PMX soot. The Raman parameters mostly sensitive to the disorder and size of aromatic rings, i.e. the $I(D)/I(G)$ ratio and the full width at half maximum (FWHM) of the G peak, exhibit the same values for the IDF and young PMX soot (Table 1). In comparison to young PMX soot, as found in previous work [45, 53], the spectrum of mature soot shows wider D and G peaks and a higher $I(D)/I(G)$ ratio (Table 1). From the $I(D)/I(G)$ ratio reported in Table 1, aromatic layer lengths of about 1nm have been evaluated [45, 53].

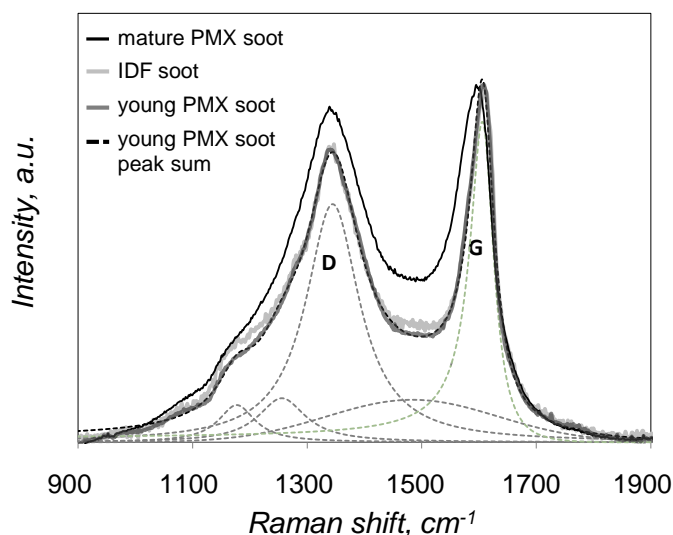


Figure 2 Raman spectra of the PMX (young and mature) and IDF soot samples. The reconstructed spectrum of young PMX soot obtained by fitting with deconvoluted peaks [51] is reported for comparison.

Also, the optical band gap values measured on the UV-Vis spectra of IDF and young PMX soot appear similar and higher (0.5-0.7eV) than that evaluated for mature PMX soot (about 0.2) (Table 1). However, such E_g values are still closer to the band gap value of graphite ($E_g=0eV$) than to the E_g values of four- to seven-ten ring PAH (>2eV), and consequently, are in contradiction with the soot structural model based on small- to medium-size PAH as main elementary units of soot [45, 47-53]. Besides, the E_g values of soot are much lower in respect to the E_g of PAH, typically detected in the organic carbon, underlining the discontinuity already found between the UV-Vis spectra of organic carbon and black carbon constituting the combustion aerosol [67]. It is also

noteworthy that such spectral discontinuity somehow corresponds to the lack of continuity in the molecular masses distribution from PAH to the first soot particles measured in sooting flames [68, 69].

The main spectral features typifying and discriminating the organic carbon from soot can be seen in Figure 3 where the UV-Vis absorption and fluorescence spectra of organic carbon (Figure 3a) and soot (Figure 3b) for the IDF sample are reported as a function of the wavelength. The UV-Vis absorption and fluorescence spectra of organic carbon show the fine structure typical of PAH [46, 70] whereas soot exhibit a broad shape of the UV-Vis spectrum more shifted toward the visible in comparison to the organic carbon. As regards soot, only a weak green fluorescence pertaining just to the <20nm size fraction of soot has been observed (Figure 3b) [71,72].

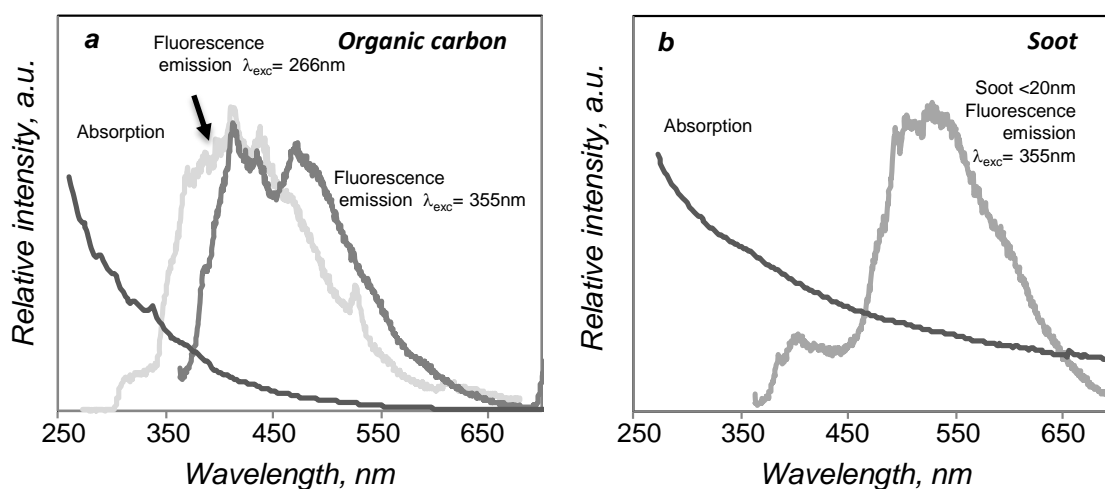


Figure 3 a) Absorption and fluorescence spectra of the organic carbon, b) absorption spectrum of soot and fluorescence of the filtered soot fraction (<20nm).

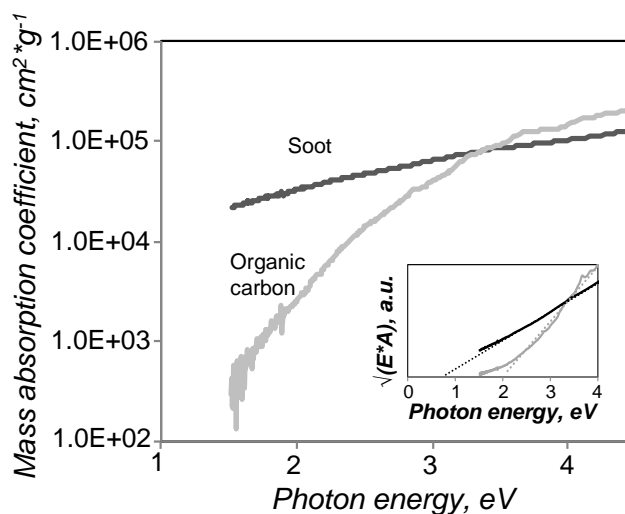


Figure 4 Mass absorption coefficient of the organic carbon and soot as a function of the photon energy, Tauc plot is shown in the inset.

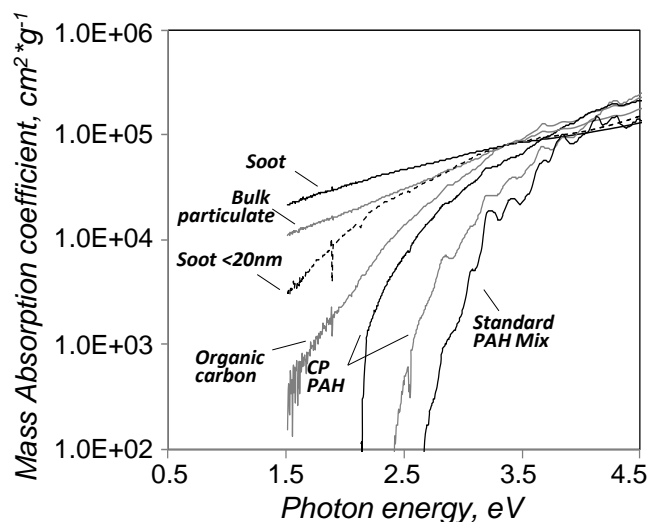


Figure 5 Mass absorption coefficient of bulk carbon particulate and relative fractions (soot, soot<20nm and organic carbon) in comparison with standard PAH and large PAH (heptane-soluble and toluene-soluble) derived from coal tar pitch (CP).

The semi-log diagram reporting the mass absorption coefficient (also defined as absorption cross section ($\text{cm}^2 \cdot \text{g}^{-1}$)) against photon energy (Figure 4) exemplifies differences between organic carbon and soot. In particular, the higher absorption mass coefficient in the UV along with the faster decrease of absorption downward into the visible-NIR of organic carbon are remarkable. These UV-Vis spectral features, along with the fine structure of both UV-Vis absorption and fluorescence spectra described above (Figure 3a), are typical of PAH [46, 70] and demonstrate the predominant molecular character of the organic carbon fraction, as confirmed by the abundance of small- and medium-size PAH components (about 50wt.%) found by GC-MS analysis of organic carbon. Nevertheless, it is noticeable that the absorption decrease for organic carbon is not as steep as in the case of standard PAH. This is shown in Figure 5 where the spectra of bulk particulate, soot and organic carbon fractions are contrasted with the spectra of two- to seven-ring standard PAH mixture (<300 u, < 24 C atoms), and large PAH (>300u, >20-24 C atoms) featuring the heptane-soluble (200-500 u) and toluene-soluble fractions (300-700 u) of a coal tar pitch (CP) [64]. In comparison to small- and medium-size PAH the broadening and shift at lower energy of the band edge for the organic carbon lead to the presumption of the presence of PAH aggregates [73].

With regards to soot, the broad band edge and the significant absorption down into the visible-NIR are clearly seen in Figures 4-5. In particular, Figure 5 elucidates the different contributions of organic carbon and soot to the absorption of bulk carbon in the visible-NIR range. Specifically,

even though soot and organic carbon equally contribute to the total mass of bulk carbon (Table 1), the component that predominantly affects the broadband edge, and hence the optical gap of the bulk particulate, is the soot fraction as below detailed. It is also noteworthy that the <20nm size fraction of soot, separated by filtration, somehow bridges organic carbon and soot, exhibiting intermediate absorption features as shown in Figure 5 where its UV-Vis absorption profile (shaded curve in Figure 5) is also reported.

A first estimate of the E04 band gap can be performed on the absorption-photon energy diagrams taking into account the fact that E04 is the energy value at which the absorption coefficient is equal to 10^4 cm^{-1} [25]. In particular, to evaluate E04 from the absorption profiles (Figures 4-5), the mass absorption coefficient ($\text{cm}^2 \cdot \text{g}^{-1}$) reported on the ordinate scale has to be multiplied by the mass density that goes from about 1.0-1.2 $\text{g} \cdot \text{cm}^{-3}$ for organic species to about 1.8 $\text{g} \cdot \text{cm}^{-3}$ for soot. Assuming a density of $1 \text{ g} \cdot \text{cm}^{-3}$, the E04 for the organic carbon, can be evaluated from Figure 5 by interception of the absorption profile on the energy axis at a mass absorption coefficient value of $10^4 \text{ cm}^2 \cdot \text{g}^{-1}$. The E04 of organic carbon is 2.4eV, consistent with the optical band gap value typical of medium-size PAH identified by GC-MS. The similarity of the E04 and Eg (around 2eV) measured on the Tauc plot ($(\alpha E)^{0.5}$ vs. energy) reported in the inset of Figure 4 demonstrates the good correlation of the optical band gap with the aromatic size of PAH components in the case of organic carbon.

As regards soot, the E04 is not assessable in the energy range examined (down to 1 eV) because of both the high density (>1.5 and up to 2 g/cm^3) and high absorption coefficient (> $10^4 \text{ cm}^2 \cdot \text{g}^{-1}$) of soot. For example, for soot density of 1.5 and 1.8 $\text{g} \cdot \text{cm}^{-3}$, the E04 should be evaluated as the interception of the soot spectrum (Figures 4-5) at the absorption cross section of about $7 \cdot 10^3$ and $5 \cdot 10^3 \text{ cm}^2 \cdot \text{g}^{-1}$, respectively, as these values correspond to the absorption coefficient threshold of 10^4 cm^{-1} required for E04 evaluation. It can be clearly seen (Figures 4-5) that the absorption coefficient of soot remains in large excess of these absorption values hindering the E04 valuation.

Just the broad and high absorption (in large excess of 10^4 cm^{-1}) of soot so far shown should exclude the attribution of soot absorption to direct transitions generally exhibited by a steeply decreasing absorption edge [74]. Consequently, for the optical band gap evaluation of soot, the application of $n=0.5$ as a coefficient in the Tauc-Davis Mott equation, valid for indirect transitions, appears to be more suitable than $n=2$, which is valid for direct transitions and used in other works to get optical band gap values more consistent with small aromatic layers [42, 51]. The best fitting of the IDF soot absorption spectrum in a wide energy range, observed in the Tauc plot reported in the inset of Figure 4, is the empirical criterion also supporting the choice of the coefficient $n=0.5$. Eventually, the Eg value of 0.7eV obtained from the Tauc plot inserted in Figure 4, is next to the E04 values

(0.5-0.7eV) which could be roughly estimated by extrapolation of the absorption coefficient of soot into the NIR range (Figure 5).

It has to be underlined that the use of E_g as an ordering parameter and as reflecting the carbon nanostructure, i.e. the size of aromatic cluster, has been found to work when the cluster model of Robertson is valid, i.e. for non-crystalline carbons having a relatively low sp^2 content [75]. Specifically, the cluster model could be inappropriate for soot falling within the class of low-hydrogen sp^2 -rich carbons (Figure 1), because the high sp^2 concentration prevents any clusters from being independent each other, and the interaction between π -systems in the solid state reduces the relevant energy gap [73]. The occurrence throughout the carbon network of some intra- or inter-particles interactions tunnelling/percolation effect [76, 77] can be presumed to occur as also suggested by the conductivity measured on flame-formed soot [78]. More insights on the optical band gap of multicomponent carbon materials as organic carbon and soot have been obtained by looking at the distribution of the main MW/size-segregated components reported in Figure 6 and obtained by SEC analysis coupled to on-line (point-by-point) UV-Vis spectroscopy.

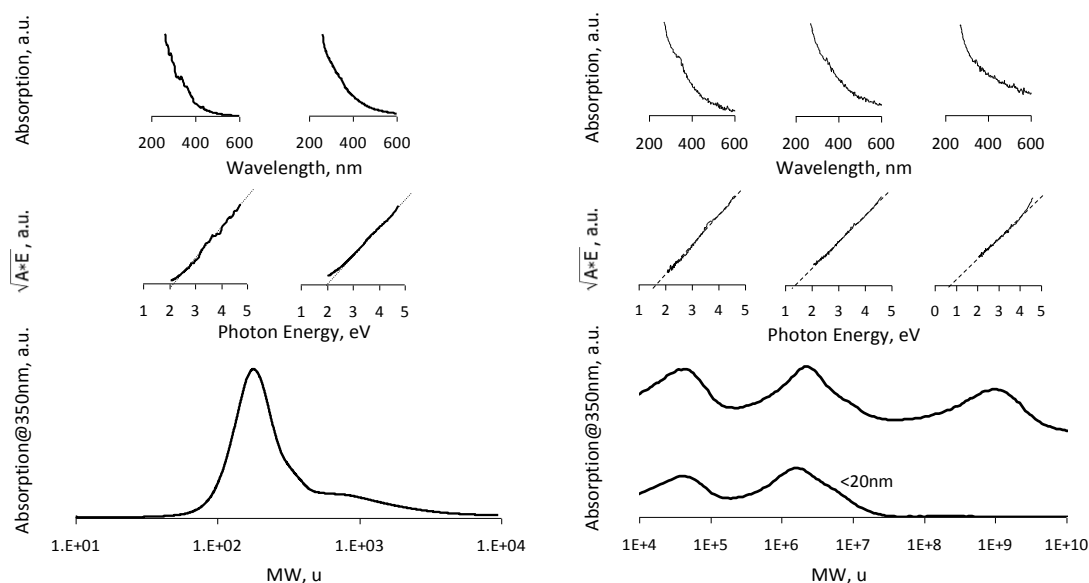


Figure 6 MW distributions of organic carbon (left panel), soot and <20nm filtered soot fraction (right panel) along with UV-Vis spectra (upper part) and Tauc plot (middle part) measured on the maximum of the MW peaks.

The MW distribution profile of the organic carbon (left part of Figure 6) shows the usual bimodal shape of flame-formed tar species [68, 72] with most of the components included in a predominant sharp peak ranging from 100 to about 400 u. A peak is observed from 600 to about 2000 u in the form of a small and broad shoulder. As observed in previous works [62, 72, 79], a relatively high

band gap, namely 2.2eV, features both components (the main peak and adjacent shoulder in the whole 100-2000 u range) of the organic carbon that is consistent with the Eg and E04 evaluated on the whole organic carbon.

Soot distribution extends into a very wide MW range (from 1E4 to 1E10 u) presenting three main and broad peaks (right panel (bottom) of Figure 6) corresponding to species of medium (1E4-1E5u), intermediate (1E5–1E7 u) and very high MW (>1E9u), in turn featured by rather low optical band gaps, 1.7, 1.3 and 0.7eV, respectively.

The optical band gap and MW data of organic carbon and soot are summarized in Table 2, which also reports the size (diameter) of the molecules and/or particles evaluated by considering a spherical shape and attributing a density of 1.2, 1.3, 1.5 and 1.8 g/cm³ at increasing MW. The last peak (> 1E9 u) of the MW/size soot distribution (Figure 6) corresponds to large size (100-200 nm) components; hence it should correspond to larger soot particles/aggregates in which size effects [80] and/or interparticle tunneling/percolation [76,77] can be responsible for the lowest Eg (0.7eV). In spite of the relatively low abundance, as compared to the other peaks (Figure 6, right panel, bottom), large soot particles/aggregates appear to be responsible for the low Eg measured on the raw soot sample. Such aggregates are completely removed not only by microfiltration on 20 nm filters, as can be seen in the bottom part of Figure 3 (right panel) reporting the MW distribution of the <20nm soot fraction, but also on 100 nm porosity filters which showed to be highly efficient (>95%) for the removal of these aggregates. All size data obtained by SEC and filtration suggest a critical size for soot particle aggregation in the 100-200 nm range, in agreement with the size range measured for soot dispersions by laser granulometry [61, 81].

It can be also concluded that the contribution of the soot and organic carbon components with higher Eg (>1.3 eV) pertains to species/particles much below 20nm and is submerged when in mixture with larger particles and/or soot aggregates.

Table 2. Optical band gap, molecular weight and bulk diameter of organic carbon and soot fractions of IDF soot

Optical band gap, eV	MW, u	"Bulk" Diameter, nm
2.2	1.0E+02-2.0E+03	0.66-1.38
1.7	1.0E+05	6.1
1.3	8.0E+06	26
0.7	4.0E+09	190

In other words, few traces of large soot particles/ aggregates contribute to most of the absorption in the whole UV-Vis range and are enough to reduce the E_g of soot and bulk carbon to the rather low values observed.

In summary, it can be inferred that the optical band gap of soot, and more generally of aromatic sp^2 -rich carbons, cannot be directly related to the aromatic layers constituting the basic units (nanostructure) of soot particles. Instead, the low optical band gap of both young and mature soot can be mainly ascribed to the soot macrostructure represented by large soot particles and/or aggregates. This is a finding which, if confirmed in other more significant flame conditions, could be relevant to the study of soot formation especially for the interpretation and modelling of soot inception and growth indicating that soot particle aggregation is a phenomenon not separated in time from particle nucleation [82-84]. Actually, in dependence on the temperature and species concentration, different particle evolution processes have been nicely suggested to simultaneously occur in coflow diffusion flames [85]. The analysis and the interpretation of the optical band gap reported in this work further supports the soot carbonization process suggested by Reilly [86] instead of the classical step-by-step evolution (from inception to aggregation) of soot particles [87]. Further work is, however, planned to be done in nearly-sooting flame conditions where the occurrence of soot aggregation and growth should be limited.

4. Conclusions

The chemical and spectroscopic features of bulk carbon (soot plus organic carbon) sampled downstream of an ethylene IDF were analyzed with the specific aim of inferring the value of the optical band gap as signature of the nanostructure of highly disordered sp^2 -rich carbons.

The chemical and spectroscopic properties of IDF soot and in particular, the H/C ratio, the relative amount of organic carbon, the absorption coefficient and Raman parameters were found to be consistent with those of young soot sampled in a premixed flame.

Accordingly with the discontinuity typically found between the molecular masses of PAH precursors and soot, the smaller extension and steeper decrease of the absorption of organic carbon were observed in comparison to soot. The Tauc plot was found to be suitable for the analysis of the optical band gap of organic carbon giving out values (around 2eV) consistent with the average size of the main PAH components. Likewise, the broad and high absorption of soot (in large excess of 10^4 cm^{-1}) and the empirical criterion of the best fitting of the IDF soot absorption spectrum in a wide energy range led to individuate the Tauc plot as the more suitable for the optical band gap evaluation of soot.

In spite of all chemical and spectroscopic properties typical of young soot, IDF soot exhibited a low optical band gap ($<0.7\text{eV}$), nearest to graphite than to PAH, contradicting the hypothesis of small- to medium-size PAH as main basic units of soot. However, a such low optical band gap was found to be predominantly associated to 100-200nm size aggregates (even few) of soot particles, whereas the contribution of species with the higher optical band gap, ranging from about 1 to 2eV, pertained to the species/particles below 20nm, and was completely obscured when in mixture with soot aggregates. This finding suggests that the optical band gap evaluation for sp^2 -rich disordered carbons as soot is mostly affected by their macrostructure in terms of particle/aggregates size, probably because of the interparticle tunnelling/percolation.

Besides the implications on the meaning of optical band gap for highly disordered sp^2 -rich carbons, it is quite remarkable that the optical band gap analysis reported in this work would be useful for inferring specific aspects of the different soot formation mechanisms occurring in diverse combustion configurations.

Acknowledgments

This work was supported by Accordo di Programma CNR-MSE Ricerca di Sistema Elettrico.

References

- 1 Negri F, Castiglioni C, Tommasini M, Zerbi G. A computational study of the Raman spectra of large Polycyclic Aromatic Hydrocarbons: toward molecularly defined subunits of graphite. *J. Phys. Chem. A* 2002; 106:3306-3317.
- 2 Müllen K, Antonietti M, Carbon materials with a kick!. *Macromol. Chem. Phys.* 2012; 213: 999–1000.
- 3 Monthieux M. Structures, textures, and thermal behaviour of polyaromatic solids. In: Setton R, Bernier P, Lefrant S, editors. *Carbon Molecules and Materials*, London: Taylor & Francis; 2002, p.127-177.
- 4 Bianco A, Cheng HM, Enoki T, Gogotsi Y, Hurt RH, Koratkar N, et al. All in the graphene family – a recommended nomenclature for two-dimensional carbon materials. *Carbon* 2013; 65:1–6.
- 5 Oberlin A, Bonnamy S. A realistic approach to disordered carbons. In: Radovic LR, editor. *Chemistry and physics of carbon*, vol. 31, CRC Press; 2013, p. 1-83.
- 6 Lighty JS, Veranth JM, Sarofim AF. Combustion aerosols: factors governing their size and composition and implications to human health. *J. Air & Waste Manage. Assoc.* 2000; 50:1565-618.
- 7 Bond TC, Doherty SJ, Fahey DW, Forster PM, Bernsten T, Deangelo BJ, et al. Bounding the role of black carbon in the climate system: A scientific assessment. *J. Geophys. Res. Atmos.* 2013; 118:5380-552.
- 8 Bond TC, Bergstrom RW. Light Absorption by Carbonaceous Particles: An Investigative Review. *Aerosol Science and Technology* 2006; 40:27-67.
- 9 Shaddix CR, Williams TC. Soot: Giver and Taker of Light. *American Scientist* 2007; 95:232-9.
- 10 Mennella V, Colangeli L, Bussoletti E, Merluzzi P, Monaco G, Palumbo P, et al. Laboratory experiments on cosmic dust analogues: the structure of small carbon grains. *Planet. Space Sci.* 1995; 43:1217-21.

- 11 Jäger C, Krasnokutski S, Staicu A, Huisken F, Mutschke H, Henning Th, et al. Identification and Spectral Properties of Polycyclic Aromatic Hydrocarbons in Carbonaceous Soot Produced by Laser Pyrolysis. *ApJS* 2006; 166: 557-566;
- 12 Carpentier Y, Féraud G, Dartois E, Brunetto R, Charon E, Cao AT, et al. Nanostructuring of carbonaceous dust as seen through the positions of the 6.2 and 7.7 μm AIBs. *A&A* 2012, 548:A40.
- 13 Millikan RC. Optical Properties of Soot. *J. Opt. Soc. Am.* 1961; 51:698-9.
- 14 Bonne U, Wagner HGg. Untersuchung des Reaktionsablaufs in fetten Kohlenwasserstoff-Sauerstoff-Flammen II. Versuche an rußenden Acetylen-Sauerstoff-Flammen bei niedrigem Druck. *Berichte der Bunsengesellschaft für physikalische Chemie* 1965; 69:20-35.
- 15 D'Alessio A, Beretta F, Venitozzi C. Optical Investigations on Soot Forming Methane-Oxygen Flames. *Combust. Sci. Tech.* 1972; 5:263-72.
- 16 Wersborg BL, Fox LK, Howard JB. Soot concentration and absorption coefficient in a low-pressure flame. *Comb. Flame* 1975, 24:1-10.
- 17 Apicella B, Alfè M, Barbella R, Tregrossi A, Ciajolo A. Aromatic structures of carbonaceous materials and soot inferred by spectroscopic analysis. *Carbon* 2004, 42:1583-9.
- 18 Alfè M, Apicella B, Rouzaud JN, Tregrossi A, Ciajolo A. The effect of temperature on soot properties in premixed methane flames. *Comb. Flame* 2010; 157:1959-65.
- 19 Russo C, Alfè M, Rouzaud JN, Stanzione F, Tregrossi A, Ciajolo A. Probing structures of soot formed in premixed flames of methane, ethylene and benzene flames. *Proc. Comb. Inst.* 2013; 34:1885-92.
- 20 Cleon G, Amodeo T, Faccinnetto A, Desgroux P. Laser induced incandescence determination of the ratio of the soot absorption functions at 532 nm and 1064 nm in the nucleation zone of a low pressure premixed sooting flame. *Appl Phys B* 2011; 104:297–305.
- 21 López-Yglesias X, Schrader PE, Michelsen HA. Soot maturity and absorption cross sections. *Journal of Aerosol Science* 2014; 75:43-64.
- 22 Tauc J, Grigorovici R, Vancu A. Optical Properties and Electronic Structure of Amorphous Germanium. *Phys. Status Solidi B* 1966; 15:627-37.

- 23 Mott NF, Davis EA. *Electronic Processes in Non-Crystalline Materials* 2nd Edition. Oxford: Clarendon Press; 1979.
- 24 Robertson J, O'Reilly EP. Electronic and atomic structure of amorphous carbon. *Phys. Rev B* 1987; 35:2946-57.
- 25 Robertson J, Hard amorphous (diamond-like) carbons. *Progress in Solid State Chemistry* 1991; 21:199-333.
- 26 Delhaes P. *Carbon-based Solids and Materials*. Wiley Online Library, DOI: 10.1002/9781118557617; 2013.
- 27 Jacob W, Moller W. On the structure of thin hydrocarbon films. *App. Phys. Lett.* 1993; 63:1771-3.
- 28 Robertson J. Gap states in diamond-like amorphous carbon. *Philosophical Magazine Part B* 1997; 76:335-50.
- 29 Robertson J. Diamond-like amorphous carbon. *Materials Science and Engineering: R: Reports* 2002; 37:129-281.
- 30 Ferrari AC, Robertson J. Interpretation of Raman spectra of disordered and amorphous carbon. *Physical Review B* 2000; 61:14095-107.
- 31 Dasgupta D, De Martino C, Demichelis F, Tagliaferro A, The role of π and π^* gaussian-like density of states bands in the interpretation of the physical properties of a-C and a-C:H films. *J. of Non-Crystalline Solids* 1993; 164-166:1147-50.
- 32 Llamas-Jansa I, Jäger C, Mutschke H, Henning Th. Far-ultraviolet to near-infrared optical properties of carbon nanoparticles produced by pulsed-laser pyrolysis of hydrocarbons and their relation with structural variations. *Carbon* 2007; 45:1542-57.
- 33 Jäger C, Huisken F, Mutschke H, Llamas Jansa I, Henning Th. Formation of PAHs and Carbonaceous Solids in Gas-Phase Condensation Experiments. *The Astrophysical Journal* 2009; 696:706-12.
- 34 Schnaiter M, Horvath H, Mohler O, Naumann KH, Saathoff H, Schock OW. UV-VIS-NIR spectral optical properties of soot and soot-containing aerosols. *Aerosol Science* 2003; 34:1421-44.

- 35 Schnaiter M, Gimmler M, Llamas I, Linke C, Jäger C, Mutschke H. Strong spectral dependence of light absorption by organic carbon particles formed by propane combustion. *Atmospheric Chemistry and Physics* 2006; 6:2981-90.
- 36 Compagnini G, Zammit U, Madhusoodanan KN. Disorder and absorption edges in ion-irradiated hydrogenated amorphous carbon films. *Phys. Rev. B* 1995; 51:11168-71.
- 37 Minutolo P, Gambi G, D'Alessio A. The optical band gap model in the interpretation of the UV-visible absorption spectra of rich premixed flames. *Symposium (International) on Combustion* 1996. 26:951-7.
- 38 Tregrossi A, Ciajolo A. Spectral Signatures of Carbon Particulate Evolution in Methane Flames. *Combust. Sci. Tech.* 2010; 182:683-91.
- 39 Russo C, Stanzione F, Alfè M, Ciajolo A, Tregrossi A. Spectral Analysis in the UV-Visible Range for Revealing the Molecular Form of Combustion-Generated Carbonaceous Species. *Combust. Sci. Tech.* 2012; 184:1291-31.
- 40 Russo C, Stanzione F, Ciajolo A, Tregrossi A. Study on the contribution of different molecular weight species to the absorption UV-Visible spectra of flame-formed carbon species. *Proc. Comb. Inst.* 2013; 34:3661-8.
- 41 Miller JH, Herdman JD, Green CDO, Webster EM, Experimental and computational determinations of optical band gaps for PAH and soot in a N₂-diluted, ethylene/air non-premixed flame. *Proc. Comb. Inst.* 2013; 34: 3669-75.
- 42 Adkins EM, Miller JH. Extinction measurements for optical band gap determination of soot in a series of nitrogen-diluted ethylene/air non-premixed flames. *Phys Chem Chem Phys.* 2015; 17:2686-95.
- 43 Commodo M, Tessitore G, De Falco G, Bruno A, Minutolo P, D'Anna A. Further details on particle inception and growth in premixed flames. *Proc. Comb. Inst.* 2015; 35:1795-802.
- 44 Bond TC, Spectral dependence of visible light absorption by carbonaceous particles emitted from coal combustion. *Geophysical Research Letters* 2001; 28:4075-78.
- 45 Apicella B, Pré P, Alfè M, Ciajolo A, Gargiulo V, Russo C, et al. Soot nanostructure evolution in premixed flames by High Resolution Electron Transmission Microscopy (HRTEM). *Proc. Comb. Inst.* 2015; 35:1895-902.

- 46 Rieger R, Müllen K. Forever young: polycyclic aromatic hydrocarbons as model cases for structural and optical studies. *J. Phys. Org. Chem.* 2010; 23:315-25.
- 47 Ebert LB, Scanlon JC, Clausen CA. Combustion tube soot from a diesel fuel/air mixture: issues in structure and reactivity. *Energy & Fuels* 1988; 2:438-45.
- 48 Frenklach M, Wang H. Detailed modeling of soot particle nucleation and growth. *Symposium (International) on Combustion* 1991; 23:1559-66.
- 49 Yehliu K, Vander Wal RL, Boehman AL. A comparison of soot nanostructure obtained using two high resolution transmission electron microscopy image analysis algorithms. *Carbon* 2011; 49:4256-68.
- 50 Alfè M, Apicella B, Barbella R, Rouzaud JN, Tregrossi A, Ciajolo A. Structure–property relationship in nanostructures of young and mature soot in premixed flames. *Proc. Comb. Inst.* 2009; 32:697-704.
- 51 Botero ML, Adkins EM, Gonzalez-Calera S, Miller H, Kraft M. PAH structure analysis of soot in a non-premixed flame using high-resolution transmission electron microscopy and optical band gap analysis. *Comb. Flame* 2016; 164:250-8.
- 52 Herdman JD, Connelly BC, Smooke MD, Long MB, Miller JH. A comparison of Raman signatures and laser-induced incandescence with direct numerical simulation of soot growth in non-premixed ethylene/air flames. *Carbon* 2011; 49:5298-311.
- 53 Russo C, Ciajolo A. Effect of the flame environment on soot nanostructure inferred by Raman spectroscopy at different excitation wavelengths. *Comb. Flame* 2015; 162:2431-41.
- 54 Blevins LG, Fletcher RA, Benner BA, Steel EB, Mulholland GW. The existence of young soot in the exhaust of inverse diffusion flames. *Proc. Combust. Inst.* 2002; 29:2325-33.
- 55 Katta VR, Blevins LG, Roquemore. Dynamics of an inverse diffusion flame and its role in polycyclic-aromatic-hydrocarbon and soot formation. *Comb. Flame* 2005; 142:33-51.
- 56 Mikofski MA, Williams TC, Shaddix CR, Blevins LG. Flame height measurement of laminar inverse diffusion flames. *Combust. Flame* 2006; 146:63-72.
- 57 Mikofski MA, Williams TC, Shaddix CR, Fernandez-Pello AC, Blevins LG. Structure of laminar sooting inverse diffusion flames. *Combust. Flame* 2007; 149:463-78.

- 58 Escudero F, Fuentes A, Demarco R, Consalvi JL, Liu F, Elicer-Cortés JC, et al. Effects of oxygen index on soot production and temperature in an ethylene inverse diffusion flame. *Experimental Thermal and Fluid Science* 2016; 73:101-8.
- 59 Zhao B, Yang X, Wang J, Johnston MW, Wang H. Analysis of Soot Nanoparticles in a Laminar Premixed Ethylene Flame by Scanning Mobility Particle Sizer. *Aerosol Science & Technology* 200; 37:611-20.
- 60 Kasper M, Siegmann K, Sattler K. Evaluation of an in situ sampling probe for its accuracy in determining particle size distributions from flames. *J. Aerosol Science* 1997; 28:1569-78.
- 61 D'Anna A, Ciajolo A, Alfè M, Apicella B, Tregrossi A. Effect of fuel/air ratio and aromaticity on the molecular weight distribution of soot in premixed n-heptane flames. *Proc. Combust. Inst.* 2009; 32:803-10.
- 62 Alfè M, Apicella B, Tregrossi A, Ciajolo A. Identification of large polycyclic aromatic hydrocarbons in carbon particulates formed in a fuel-rich premixed ethylene flame. *Carbon* 2008; 46:2059-66.
- 63 Russo C, Stanzione F, Tregrossi A, Ciajolo A. Infrared spectroscopy of some carbon-based materials relevant in combustion: Qualitative and quantitative analysis of hydrogen. *Carbon* 2014; 74:127-38.
- 64 Gargiulo V, Apicella A, Stanzione F, Tregrossi A, Millan M, Ciajolo A, et al. Structural Characterization of Large Polycyclic Aromatic Hydrocarbons. Part 2: Solvent-Separated Fractions of Coal Tar Pitch and Naphthalene-Derived Pitch. *Energy & Fuels* 2016; 30:2574-83.
- 65 Müller JO, Su DS, Wild U, Schlögl R. Bulk and surface structural investigations of diesel engine soot and carbon black. *PCCP* 2007; 9:4018-25.
- 66 Knauer M, Schuste ME, Su D, Schlögl R, Niessner R, Ivleva NP. Soot structure and reactivity analysis by Raman microspectroscopy, temperature-programmed oxidation, and high-resolution transmission electron microscopy. *J. Phys. Chem. A* 2009; 113:13871-80.
- 67 Sun H, Biedermann L, Bond TC. Color of brown carbon: A model for ultraviolet and visible light absorption by organic carbon aerosol. *Geophys. Res. Lett.* 2007; 34:L17813.

- 68 Keller A, Kovacs R, Homann KH. Large molecules, ions, radicals and small soot particles in fuel-rich hydrocarbon flames. Part IV. Large polycyclic aromatic hydrocarbons and their radicals in a fuel-rich benzene–oxygen flame. *Phys. Chem. Chem. Phys.* 2000; 2:1667-75.
- 69 Homann KH, Fullerenes and Soot Formation— New Pathways to Large Particles in Flames. *Angew. Chem. Int. Ed.* 1998. 37:2434-51.
- 70 Apicella B, Ciajolo A, Tregrossi A. Fluorescence Spectroscopy of Complex Aromatic Mixtures. *Analytical Chemistry* 2004; 76:2138-43.
- 71 Alfè M, Apicella B, Barbella R, Tregrossi A, Ciajolo A. Distribution of soot molecular weight/size along premixed flames as inferred by size exclusion chromatography. *Energy & Fuels* 2007; 21:136-40.
- 72 Ciajolo A. Condensed Phases in soot formation process. In: Bockhorn H, D'Anna A, Sarofim AF, Wang H, editors. *Combustion Generated Fine Carbonaceous Particles*, Karlsruhe: KIT Scientific Publishing; 2009, p. 333-44.
- 73 Watson MD, Fechtenkötter A Müllen K. Big Is Beautiful—“Aromaticity” Revisited from the Viewpoint of Macromolecular and Supramolecular Benzene Chemistry. *Chem. Rev.* 2001; 101: 1267-300.
- 74 Pankove J. *Optical Processes in Semiconductors*. Mineola: Courier Dover Publications; 1971.
- 75 Robertson J. Recombination and photoluminescence mechanism in hydrogenated amorphous carbon. *Physical Review B* 1996; 53:16302-5.
- 76 Fanchini G, Ray SC, Tagliaferro A. Optical properties of disordered carbon-based materials. *Surface and Coatings Technology* 2002; 151 –152: 233-41.
- 77 Theye ML, Paret V. Spatial organization of the sp^2 -hybridized carbon atoms and electronic density of states of hydrogenated amorphous carbon films. *Carbon* 2002; 40:1153-66.
- 78 De Falco G, Commodo M, Bonavolontà C, Pepe GP, Minutolo P, D'Anna A. Optical and electrical characterization of carbon nanoparticles produced in laminar premixed flames. *Combust. Flame* 2014; 161:3201-10.

- 79 Sirignano M, Alfè M, Tregrossi A, Ciajolo A, D'Anna A. Experimental and modeling study on the molecular weight distribution and properties of carbon particles in premixed sooting flames. *Proceedings of the Combustion Institute* 2011; 33:633-40.
- 80 Rossetti, R.; Nakahara, S.; Brus, L. E. Quantum size effects in the redox potentials, resonance Raman spectra, and electronic spectra of CdS crystallites in aqueous solution *J. Chem. Phys.* 1983,79, 1086
- 81 Senneca O, Apicella B, Heuer S, Schiemann M, Scherer V, Stanzione F, et al. Effects of CO₂ on submicronic carbon particulate (soot) formed during coal pyrolysis in a drop tube reactor. *Comb. Flame* 2016; 172:302-8.
- 82 Frenklach M. Reaction mechanism of soot formation in flames. *Phys Chem Chem Phys.* 2002; 4:2028-37.
- 83 Di Stasio S. Electron microscopy evidence of aggregation under three different size scales for soot nanoparticles in flame. *Carbon* 2001; 39:109-18.
- 84 Vander Wal RL. Soot precursor material: Visualization via simultaneous IIF-LII and characterization via tem- Symposium (International) on Combustion 1996. 26: 2269-75.
- 85 Kholghy M, Saffaripour M, Yip C, Thomson MJ. The Evolution of Soot Morphology in an Atmospheric Laminar Coflow Diffusion Flame of a Surrogate for Jet A-1. *Comb. Flame* 2013; 160:2119-30.
- 86 Reilly PTA, Gieray RA, Whitten WB, Ramsey JM. Direct observation of the evolution of the soot carbonization process in an acetylene diffusion flame via real-time aerosol mass spectrometry. *Comb. Flame* 2000; 122:90-104.
- 87 Lahaye J. Particulate carbon from the gas phase. *Carbon* 1992; 30:309-14.